

Ternary Pt/Rh/SnO₂ electrocatalysts for oxidizing ethanol to CO₂

A. Kowal^{1*}, M. Li¹, M. Shao^{1*}, K. Sasaki¹, M. B. Vukmirovic¹, J. Zhang^{1*}, N. S. Marinkovic², P. Liu¹, A. I. Frenkel³ and R. R. Adzic^{1†}

Ethanol, with its high energy density, likely production from renewable sources and ease of storage and transportation, is almost the ideal combustible for fuel cells wherein its chemical energy can be converted directly into electrical energy. However, commercialization of direct ethanol fuel cells has been impeded by ethanol's slow, inefficient oxidation even at the best electrocatalysts^{1,2}. We synthesized a ternary PtRhSnO₂/C electrocatalyst by depositing platinum and rhodium atoms on carbon-supported tin dioxide nanoparticles that is capable of oxidizing ethanol with high efficiency and holds great promise for resolving the impediments to developing practical direct ethanol fuel cells. This electrocatalyst effectively splits the C–C bond in ethanol at room temperature in acid solutions, facilitating its oxidation at low potentials to CO₂, which has not been achieved with existing catalysts. Our experiments and density functional theory calculations indicate that the electrocatalyst's activity is due to the specific property of each of its constituents, induced by their interactions. These findings help explain the high activity of Pt–Ru for methanol oxidation and the lack of it for ethanol oxidation, and point to the way to accomplishing the C–C bond splitting in other catalytic processes.

Developing electrocatalysts for ethanol oxidation to CO₂ that break the C–C bond has been a major challenge in electrocatalysis. The existing electrocatalysts can accomplish that only at extreme positive potentials^{3–6}, which renders them unsuitable for direct ethanol fuel cells⁷. *In situ* infrared reflection-absorption spectroscopy^{8,9} (IRRAS) and differential electrochemical mass spectrometry¹⁰ have shown that acetaldehyde and acetic acid are the main reaction products. Here, we describe PtRhSnO₂, a ternary electrocatalyst capable of oxidizing ethanol to CO₂. For its synthesis, we developed a cation-adsorption-reduction-galvanic-displacement synthetic method (see Supplementary Information, S1) that facilitates the controllable deposition of metal atoms on oxide surfaces¹¹. Using this method, we placed Pt and Rh atoms on SnO₂ to synthesize the ternary PtRhSnO₂ electrocatalyst.

Figure 1a shows a considerably higher current of ethanol oxidation, that is, higher activity, for the ternary PtRhSnO₂/C electrocatalyst than that of PtSnO₂/C, highlighting the importance of the Rh component. Further tests showed that the activity of RhSnO₂/C (no Pt) electrocatalysts was low. Thus, both Pt and Rh at SnO₂ are necessary for an active electrocatalyst. Figure 1b shows the comparison between PtRhSnO₂/C electrocatalyst and a commercial Pt/C electrocatalyst lacking Rh and SnO₂ in quasi-steady-state conditions at a sweep rate of 1 mV s⁻¹. At 0.3 V, the

current density for the ternary electrocatalyst is more than two orders of magnitude larger than that of the commercial Pt/C electrocatalyst. All potentials are given with respect to a reversible hydrogen electrode (RHE). The Tafel slope of ~120 mV can be obtained from that plot, indicating that the first charge transfer is the rate-determining step. Figure 1c shows a very high rate of ethanol oxidation of the PtRhSnO₂/C electrocatalyst (current density of 7.5 mA cm⁻²) at 60 °C, namely, a temperature close to that at which direct ethanol fuel cells operate (60–80 °C) at the potential of 0.3 V. At this same potential, PtRu/C, the common electrocatalyst for ethanol oxidation, has a negligible current density. The chronoamperometric measurements (Fig. 1d) confirm the high activity of the PtRhSnO₂/C electrocatalyst, which is ~100 times higher than the corresponding activity of Pt/C.

We determined the structural and electronic properties of PtRhSnO₂ electrocatalyst and their potential dependence using *in situ* X-ray absorption near-edge structure (XANES) and extended X-ray absorption fine structure (EXAFS) techniques, and combined them with data obtained by transmission electron microscopy (TEM) and inductively coupled plasma (ICP) analysis. Figure 2a,c shows the Rh K-edge and Pt L3-edge XANES spectra for PtRhSnO₂/C, respectively obtained in the potential region from 0.21 to 1.11 V in 1 M HClO₄ solution. The main absorption peaks at the Rh and Pt edges have a very small potential dependence, indicating that the surfaces are only slightly oxidized, unlike the process that occurs with the pure Rh phase. It is likely that OH, which is present on the SnO₂ surface in aqueous solutions, causes a shift in surface oxidation of Rh and Pt (Rh– or Pt–OH formation) to positive potentials induced by the OH–OH repulsion¹². The adsorption and dissociation of H₂O on SnO₂ have been verified in a number of studies^{13,14}. In general, on oxide surfaces, water molecules are adsorbed on metal ions with the transfer of one of the protons to a neighbouring oxygen atom. A 'carpet' of OH groups mediates the interaction between the oxide surface and the environment. Oxide surfaces behave as non-polarizable interfaces in which the electrical state is controlled by the solution's pH and the effect of the electrode potential is negligible even for conductive oxides¹⁵.

EXAFS spectroscopy measurements with input from TEM studies provided detailed information on the intra-particle composition and degree of alloying of Pt and Rh. Figure 2b,d shows the Fourier-transform magnitudes of the EXAFS data that correspond to the above XANES spectra at 0.41 V and theoretical signals that were fitted to the Rh K-edge and Pt L3-edge data concurrently, by applying physically reasonable constraints^{16,17}.

¹Department of Chemistry, Brookhaven National Laboratory, Upton, New York 11973, USA, ²Department of Chemical Engineering, University of Delaware, Newark, Delaware 19716, USA, ³Physics Department, Yeshiva University, New York, New York 10016, USA. *Present addresses: Institute of Catalysis and Surface Chemistry, Krakow, and Institute of Non-ferrous Metals Department, Poznan, CLAI0, Poznan PL-30216, Poland (A.K.); UTC Power Corporation, South Windsor, Connecticut 06074, USA (M.S.); General Motors Corporation, Honeoye Falls, New York 14472, USA (J.Z.). †e-mail: adzic@bnl.gov.

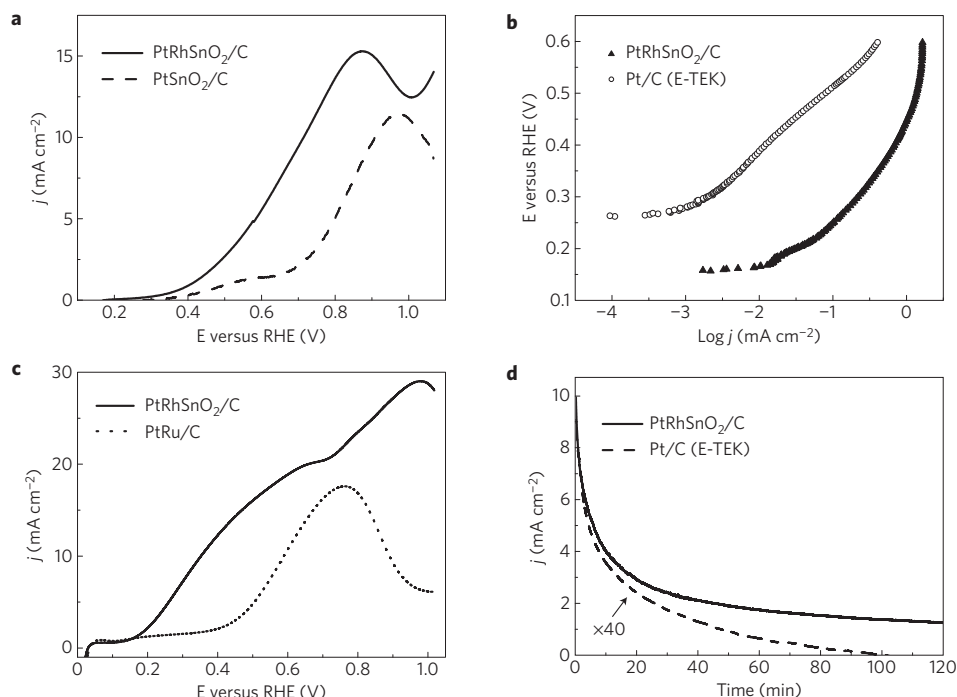


Figure 1 | Current-potential and current-time polarization curves comparing the activity of PtRhSnO₂/C with several other catalysts for ethanol oxidation. **a**, Polarization curves for the oxidation of ethanol on PtRhSnO₂/C and PtSnO₂/C thin-film electrocatalysts deposited on a glassy carbon electrode. Electrocatalyst compositions: PtRhSnO₂/C – ~30 nmol Pt, 8 nmol Rh and 60 nmol SnO₂; PtSnO₂/C – ~30 nmol Pt and 60 nmol SnO₂; electrode surface area is 0.2 cm²; 0.1 M HClO₄; 0.2 M ethanol; sweep rate is 50 mV s⁻¹. **b**, Quasi-steady-state polarization curves for the oxidation of ethanol on PtRhSnO₂/C and Pt/C (20% Pt on C E-TEK) electrocatalysts on a glassy carbon electrode. Electrocatalyst compositions: PtRhSnO₂/C – 25 nmol Pt, 16 nmol Rh and 25 nmol SnO₂; Pt/C – 25 nmol Pt; electrode surface area is 0.2 cm²; 0.1 M HClO₄; 0.5 M ethanol; sweep rate is 1 mV s⁻¹. **c**, Polarization curves for electrocatalysts for the oxidation of ethanol on PtRhSnO₂/C and PtRu/C (20% PtRu with 1:1 atomic ratio on C E-TEK) at 60 °C. Electrocatalyst compositions: PtRhSnO₂/C – 25 nmol Pt, 5 nmol Rh and 20 nmol SnO₂; PtRu/C: 25 nmol Pt, Ru: 25 nmol, other conditions as in **a**. **d**, Chronoamperometry measurements of ethanol oxidation at 0.45 V on PtRhSnO₂/C and Pt/C catalysts at 60 °C in 0.5 M C₂H₅OH in 0.1 M HClO₄. The current for Pt/C is multiplied by 40.

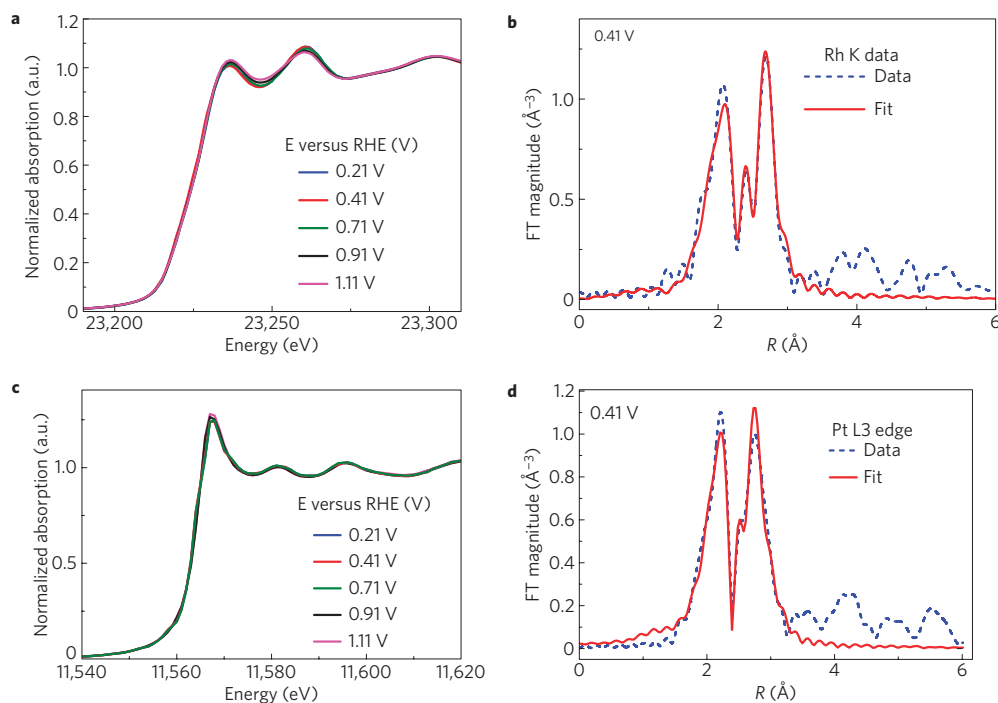


Figure 2 | In situ XANES and EXAFS spectra for determining the structural and electronic properties of PtRhSnO₂. **a–d**, XANES spectra (**a,c**) and Fourier-transform magnitudes (**b,d**) of the Rh K-edge (**a,b**) and Pt L3-edge (**c,d**) for the PtRhSnO₂/C electrocatalyst in 1 M HClO₄ solution as a function of potential. Potential settings for **a,c** are indicated in the graphs.

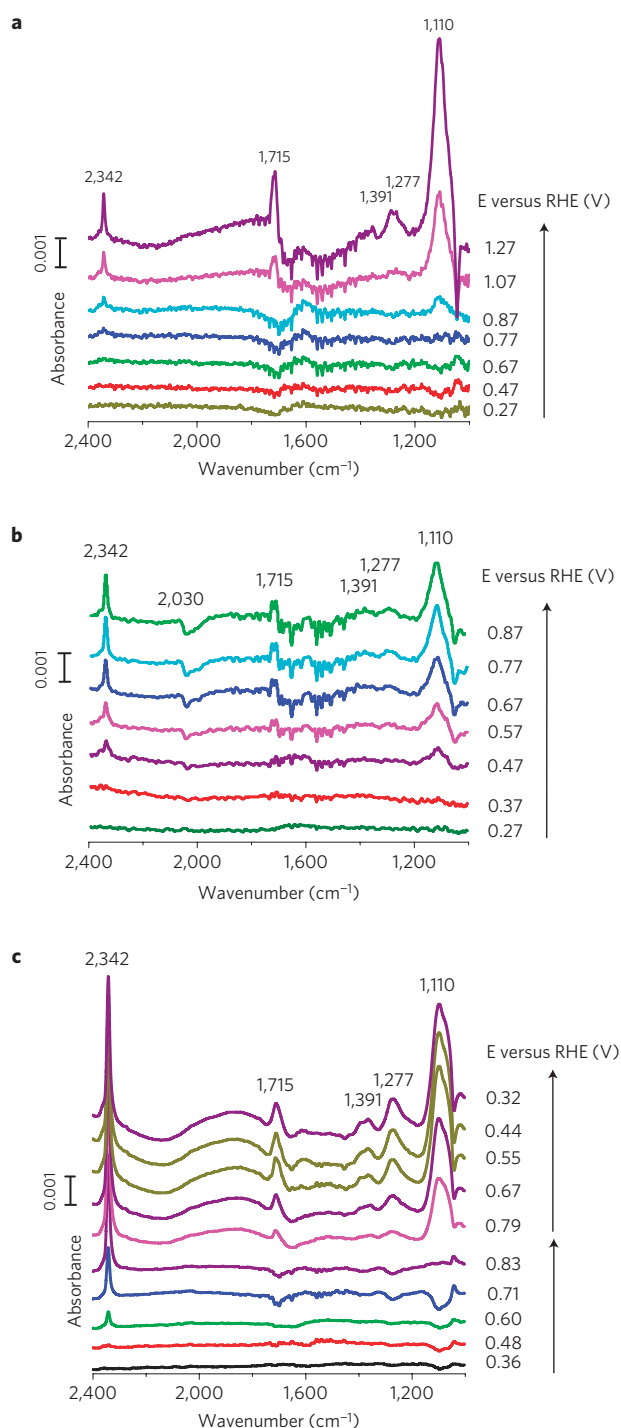


Figure 3 | *In situ* IRRAS spectra for identifying the intermediates and products of ethanol oxidation on several electrocatalysts. **a–c**, *In situ* IRRAS spectra recorded during ethanol electrooxidation on the Pt(111) electrode (**a**), on RhSnO₂/Pt(111) consisting of clusters equivalent to 2 ML of SnO₂ and 0.5 ML Rh on a Pt(111) electrode surface (**b**) and PtRhSnO₂/C in a 0.2 M ethanol in 0.1 M HClO₄ solution (**c**). 128 interferograms (resolution 8 cm⁻¹) were collected and added into each spectrum.

The results of fittings in the *k*-space of Rh and Pt edges are shown in (Fig. 2, Supplementary Information, S2). Measurements of metal–metal (Rh–Pt and Pt–Rh) coordination numbers $N_{\text{Rh–Pt}}$ and $N_{\text{Pt–Rh}}$ enabled us to obtain the average composition of the nanoparticles: $x(\text{Pt})/x(\text{Rh}) = N_{\text{Rh–Pt}}/N_{\text{Pt–Rh}} = 2.1 \pm 0.3$, in reasonably good agreement with the ICP data $x(\text{Pt})/x(\text{Rh}) = 1.5 \pm 0.2$. The absolute

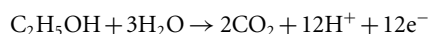
values of these coordination numbers indicate the same size range (1–3 nm) as obtained by TEM (see Supplementary Information, S2). The obtained Pt–metal and Rh–metal coordination numbers $N_{\text{Pt–M}} = N_{\text{Pt–Pt}} + N_{\text{Pt–Rh}}$ and $N_{\text{Rh–M}} = N_{\text{Rh–Rh}} + N_{\text{Rh–Pt}}$ have similar values (9.5 ± 0.8 and 10.8 ± 0.8 , respectively), consistent with homogeneous distribution of Pt and Rh throughout the particles. In addition, as the $N_{\text{Pt–Pt}}/N_{\text{Pt–Rh}}$ and $N_{\text{Rh–Pt}}/N_{\text{Rh–Rh}}$ ratios were found to be consistent, within the uncertainties, with the bulk ratios of Pt and Rh concentrations obtained independently by EXAFS and ICP, we conclude that the Pt and Rh formed a quasi-random alloy. Further independent evidence towards that conclusion is the similarity between the Pt–Pt, Pt–Rh and Rh–Rh bond lengths found by our EXAFS analysis: $2.743 \pm 0.003 \text{ \AA}$, $2.725 \pm 0.004 \text{ \AA}$, and $2.705 \pm 0.005 \text{ \AA}$, respectively, that is, characterized by a much smaller spread than between pure Pt (2.775 Å) and Rh (2.689 Å).

We used *in situ* IRRAS to identify the intermediates and products of ethanol oxidation. First, we synthesized the model catalyst using a Pt(111) surface as the support for Rh and SnO₂. Figure 3a,b illustrates the different key features of the recorded spectra for the bare Pt(111) and RhSnO₂/Pt(111) electrode surfaces. The positive potential-dependent peak near 2,342 cm⁻¹ is the signature peak for the asymmetric stretch vibration of CO₂ that appears above 0.78 V on the Pt(111) electrode, but is already apparent above 0.30 V on the RhSnO₂/Pt(111) electrode. The presence of CO₂ indicates the successful cleavage of the C–C bond in ethanol. The Pt(111) surface is partially covered by clusters of SnO₂ and Rh, respectively equivalent to amounts of 2 monolayers (ML) and 0.5 ML. The bipolar peak at 2,030 cm⁻¹ was assigned to linearly adsorbed CO (CO_L). The band located at around 1,715 cm⁻¹ reflected the stretch vibration of the C=O bond in acetaldehyde and/or acetic acid, both of which are partial oxidation products. Considerably weaker bands occurred for acetaldehyde at 1,715 cm⁻¹ and acetic acid at 1,277 cm⁻¹ for the ternary catalyst, confirming the significant decrease of their yield. The spectra for carbon-supported PtRhSnO₂ are shown in Fig. 3c. A high activity of this electrocatalyst is reflected in strong CO₂ bands and negligible CO bands.

On platinum, the first step on adsorption of ethanol involves δ -C–H dissociation¹⁸, leading to the formation of adsorbed acetaldehyde:



Our surface-enhanced infrared measurements for Pt (ref. 19) show that the partial oxidation of ethanol generates CH₃CHO and CH₃COOH species. For the PtRhSnO₂ electrocatalyst, the generation of acetic acid is negligible (1,277 cm⁻¹), the yield of acetaldehyde is significantly decreased (1,715 cm⁻¹), and the negative-moving band for CO increases with rising potential (2,030 cm⁻¹). These data indicate that on this electrocatalyst, the C–C bond in ethanol is broken directly without going through the acetaldehyde step. The reaction predominantly involves ethanol oxidation to CO₂:



This conclusion is supported by the plots of the band intensities as a function of potential (see Supplementary Information, S4).

We carried out a density functional theory (DFT) investigation (see the Methods section) of ethanol decomposition over a model RhPt/SnO₂(110) electrocatalyst to obtain further information on this reaction, in particular on splitting the C–C bond and the roles of Rh, Pt and SnO₂. Rh, at a coverage of 1/4 ML on SnO₂(110), generates a metal chain bridging Sn at a coordinatively unsaturated site (Sn_{cus}) and oxygen at bridge sites²⁰. The binding energy corresponds, respectively, to -2.82 eV/Pt

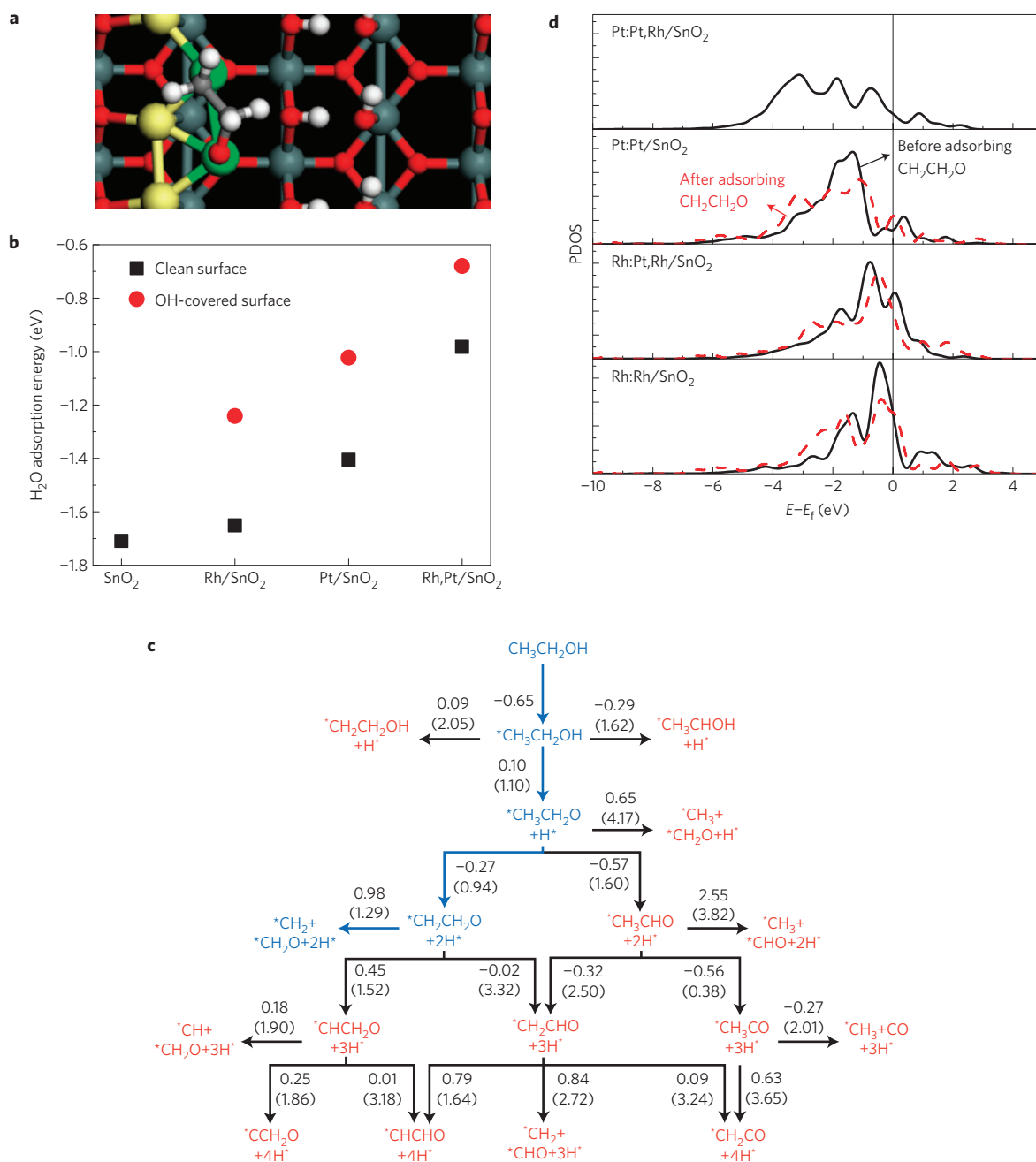
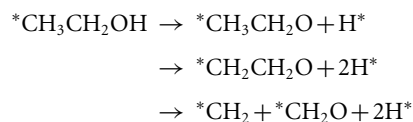


Figure 4 | DFT investigations of ethanol oxidation on a RhPt/SnO₂(110) surface. **a**, Optimized geometry of CH₂CH₂O adsorption on a RhPt/SnO₂(110) surface. (Sn: large grey; Pt: large yellow; Rh: large green; C: small grey; O: small red; H: small white.) **b**, DFT-calculated adsorption energies of water on the surfaces of SnO₂(110), Rh/SnO₂(110), Pt/SnO₂(110) and RhPt/SnO₂(110) with and without water saturating the SnO₂ sites. **c**, Calculated possible reaction pathways for the C–C bond breaking of ethanol on the RhPt/SnO₂(110) surface. The reaction energies and parenthesized barriers in the figure are expressed in electronvolts. **d**, Calculated PDOS of the *d*-state of Pt or Rh on the Rh/SnO₂(110), Pt/SnO₂(110) and RhPt/SnO₂(110) surfaces. The solid lines correspond to a bare surface, and the dashed lines represent the case after interacting with CH₂CH₂O.

atom and -2.95 eV/Rh atom. The co-deposition of Rh and Pt forms an alloy chain along a Sn_{cus} row (Fig. 4a) with the binding energy of -3.22 eV/metal atom. Figure 4a shows water strongly adsorbs on SnO₂ sites undergoing the spontaneous breakage of one of the O–H bonds. In contrast, the Pt or/and Rh sites are much less active and the water molecule stays intact. Therefore, we assume that SnO₂ sites are saturated by H₂O/OH under the electrochemical condition, thereby weakening the interaction of water with Pt or Rh, which is significant for nanoparticles containing low-coordination sites, making them available for ethanol oxidation (Fig. 4b).

Furthermore, we considered the possible reaction pathways from gaseous ethanol to C–C bond splitting. Figure 4c includes the calculated energetics for ethanol decomposition on the RhPt/SnO₂(110) surface with dissociated water saturating the oxide sites. Among all of the possibilities, the following is the optimal pathway to C–C bond breaking:



Here, all adsorbates prefer the pure Rh sites except atomic hydrogen, which favours the Rh–Pt hybrid hollow sites. Thus, ethanol decomposition on RhPt/SnO₂(110) occurs through an oxametallacyclic conformation (CH₂CH₂O, Fig. 4a) that entails direct C–C bond cleavage with a reasonable barrier of 1.29 eV. In contrast, the formation of acetaldehyde (CH₃CHO) is not favoured, having the barrier higher by 0.66 eV, and the barrier for C–C bond breaking in CH₃CHO is very high, requiring 3.82 eV (Fig. 4c). This agrees with the effect of Rh addition at the metal–gas interface, showing the preference for the CH₂CH₂O conformation^{21–23}. In addition, our calculations show that the barrier to CH₂CH₂O generation decreases in the following sequence: Pt/SnO₂ (1.53 eV) > Rh/SnO₂ (0.98 eV) > PtRh/SnO₂ (0.94 eV). Thus, the presence of Rh is essential for the formation of CH₂CH₂O. In accordance with Fig. 3, the splitting of the C–C bond does not occur through the pathway involving acetaldehyde. Its negligible coverage, and the evidence of CO involvement in the reaction, means that this catalyst facilitates a direct splitting of the C–C bond, substantiated by our DFT calculations. Spectra in Fig. 3, however, do not show evidence for oxametallacycles. The bands that are accessible under our conditions are weak ($\nu(\text{C–H})$, $w(\text{C–H}_2)$), whereas CH₂O has the C–O bond parallel to the Pt surface, which is not infrared active²⁴ and cannot be seen.

We also calculated the partial density of states (PDOS) of the *d*-state of the supported Pt and Rh atoms on SnO₂(110) before and after interacting with CH₂CH₂O to gain further information on bond formation. As Fig. 4d illustrates, the metal–CH₂CH₂O reaction is dominated by backdonation from the π orbitals of CH₂CH₂O to the *d*-orbital of the metal atoms. Accordingly, Rh obviously is a better choice to stabilize the metal–CH₂CH₂O complex than is Pt, which has a high-lying *d*-band and more unoccupied *d*-states. In addition, the mixture of Rh and Pt facilitates the occurrence of more empty states of Rh than does Rh alone on SnO₂. The strong interaction between Pt and Rh is accompanied by an electron transfer from Rh to Pt, and more *d*-states of Rh become available above the Fermi level. Concurrently, the *d*-states of Pt shift away from the Fermi level, causing a lower activity of Pt in PtRh/SnO₂ than Rh, or even Pt in Pt/SnO₂. Our calculations show that Pt in PtRh/SnO₂ weakly interacts with ethanol, and the other dissociated oxygenates and hydrocarbons. It is active only for dissociated H. Thus, the results also imply that slightly increasing the amount of Pt will empty more *d*-states of Rh, thereby improving the activity for ethanol oxidation, as inferred from our experimental data.

In summary, we successfully synthesized the ternary PtRhSnO₂/C electrocatalyst, effective in splitting the C–C bond of ethanol at room temperature, and causing its predominant oxidation to CO₂. The CO₂ generation was verified using *in situ* IRRAS. Our analyses reveal that its catalytic activity rests on the synergy between the three constituents of the electrocatalyst. Further support for synergy is afforded by similar activity of the Pt(111)/RhSnO₂ and Rh(111)/PtSnO₂ surfaces (see Supplementary Information, S2). Thus, SnO₂ by strongly adsorbing water and interacting with the Pt and Rh deposited on its surface, apparently precludes the Rh and Pt sites from reacting with H₂O to form M–OH (see the text and the XANES spectra in Fig. 2a,c), making them available for ethanol oxidation. SnO₂ with H₂O provides OH species to oxidize the dissociated CO at Rh sites, and Pt facilitates ethanol dehydrogenation. It also modifies the electronic structure of Rh to afford moderate bonding to ethanol, intermediates and products, which facilitates C–C bond breaking and, therefore, ethanol oxidation. The DFT calculations demonstrated that the oxidation of ethanol on PtRh/SnO₂ proceeds through oxametallacyclic conformation that facilitates the direct cleavage of the C–C bond at a reasonable rate. The high activity of Pt–Ru for methanol oxidation and

the lack of it for ethanol oxidation seems to be due to a high propensity of Ru to form RuOH in interaction with H₂O at potentials $E > 0.0$ V (ref. 25). This reaction cannot be suppressed in the OH–OH repulsion with SnOH, as it happens with weakly bonded RhOH. RuOH does not adsorb ethanol and cannot split the C–C bond. However, in PtRu, it efficiently oxidizes CO in methanol oxidation. The last reaction cannot be accomplished by the metallic-like Rh in PtRh/SnO₂. Thus, replacing expensive Rh should be sought in designing bimetallic and near-surface alloys that can provide adsorption and surface oxidation properties close to those of Rh.

Methods

Catalyst synthesis. The carbon-supported nanoparticle PtRhSnO₂ electrocatalyst was synthesized using a controllable deposition of metal atoms on oxide surfaces, termed the cation-adsorption-reduction-galvanic-displacement method (Patent application 2007) (further details in Supplementary Information, S1). SnO₂ nanoparticles were prepared by heating ethylene glycol solution containing SnCl₂ (ref. 26) and then were deposited on carbon Vulcan XC-72. Pb²⁺ cations were adsorbed on SnO₂ in solutions with pH ~ 11. The oxide with adsorbed Pb²⁺ was emersed from solution and Pb²⁺ was reduced electrochemically in Pb²⁺-free solution. Pb⁰ was then displaced by Pt on immersion in a Pt²⁺ solution. Rh was placed on Pt by the galvanic displacement of an underpotentially deposited Cu layer on Pt sites.

RhSnO₂/Pt(111) electrode surfaces used in the IRRAS study were prepared by placing Rh and SnO₂ nanoclusters on a Pt(111) single-crystal surface. Rh clusters, an amount equivalent to 1/2 ML, were obtained by displacing an underpotentially deposited Cu layer on Pt(111). SnO₂ clusters, an amount equivalent to 2 ML, were formed by thermal decomposition of a SnCl₄ drop on a Rh/Pt(111) surface at 200 °C.

IRRAS. *In situ* IRRAS studies were carried out with a Nicolet Nexus 670 Fourier-transform infrared spectrometer equipped with a mercury cadmium telluride detector cooled with liquid nitrogen. An unpolarized light beam was used. The spectral resolution was set to 8 cm⁻¹ and 128 interferograms were together added to each spectrum. Spectra are given in absorbance units defined as $A = -\log(R/R_0)$, where R and R_0 represent the reflected infrared intensities corresponding to the sample and reference single-beam spectrum, respectively. The reference spectrum was collected at 0.2 V in the same solution with 0.5 M ethanol and 0.1 M HClO₄. Electrodes used for the infrared study included bare Pt(111), RhSnO₂/Pt(111) and PtRhSnO₂/C nanoparticle electrocatalyst. In the last case, nanoparticles were placed on Au(111) or on Pt(111) surfaces to ensure a good current collection and reflectivity. A very dilute Nafion solution was used to immobilize the nanoparticles. A ZnSe hemisphere was used as the infrared window.

X-ray absorption spectroscopy. *In situ* X-ray absorption spectroscopy (XAS) measurements were conducted at K-edges for Rh and Sn, and the L3-edge for Pt at beamline X18 B at the National Synchrotron Light Source, Brookhaven National Laboratory. The beam was detuned by 20% at the Pt L3-edge to reject higher harmonics; no detuning is necessary for Rh and Sn K-edges. The XAS data were collected up to about 1,530 eV past the absorption edge, corresponding to the wavenumbers of 20 Å⁻¹. Three detectors, for the incident, transmitted and reference beam intensity measurements were used; the last detector serving as a reference for absolute energy calibration and alignment. The XAS data were collected with the storage ring operating at 2.8 GeV and an electron current between 110 and 350 mA.

Carbon-supported Rh/Pt/SnO₂ nanoparticles were pressed and sealed in a Plexiglas cell using Kapton tape. *In situ* XAS studies were carried out using a spectro-electrochemical cell, designed for spectroscopic measurements in both fluorescence and transmission mode. We used transmission data for all edges. Details of the cell are given elsewhere (see, for instance, the Synchrotron Catalysis Consortium web page: <<http://www.yu.edu/scc/>>). XAS spectra were collected at specific potentials between hydrogen and oxygen evolution regions in steps of 0.1 V and steady-state potential mode, allowing ~2 min for current stabilization. The XAS data were processed and fitted using Athena and Artemis analysis packages. The Pt and Rh edge data were fitted simultaneously by setting the bond distance of $R_{\text{Pt–Rh}} = R_{\text{Rh–Pt}}$, and constraining the parameters of S_0^2 to the values determined from fitting the reference metal foils (Pt and Rh). Only the data range 1.2–3.2 Å was fitted with the first-shell single scattering paths.

DFT calculation. The unrestricted DFT calculations were carried out using the DMol3 code by Delley²⁷. The ionic cores were described by effective core potentials, with a numerical basis set and the generalized gradient approximation revised version of the Perdew–Burke–Ernzerhof functional to describe the exchange and correlation. SnO₂(110) was modelled by means of the supercell approach with three O–Sn–O layer slabs and an 11 Å vacuum between the slabs. The top O–Sn–O

layer of SnO₂ substrate, the Rh and Pt atoms on the surface and the adsorbates were allowed to fully relax. Transition states were identified using the combination of synchronous transit methods and an eigenvector following ref. 27.

Received 23 September 2008; accepted 16 December 2008;
published online 25 January 2009

References

1. Lamy, C., Rousseau, S., Belgsir, E. M., Coutanceau, C. & Leger, J.-M. Recent progress in the direct ethanol fuel cell: Development of new platinum-tin electrocatalysts. *Electrochim. Acta* **49**, 3901–3908 (2004).
2. Antolini, E. Catalysts for direct ethanol fuel cells. *J. Power Sources* **170**, 1–12 (2007).
3. Mann, J., Yao, N. & Bocarsly, A. B. Characterization and analysis of new catalysts for a direct ethanol fuel cell. *Langmuir* **22**, 10432–10436 (2006).
4. Lai, S. C. S. & Koper, M. T. M. Electro-oxidation of ethanol and acetaldehyde on platinum single-crystal electrodes. *Faraday Discuss.* **140**, 399–416 (2008).
5. Tarnowski, D. J. & Korzeniewski, C. Effects of surface step density on the electrochemical oxidation of ethanol to acetic acid. *J. Phys. Chem. B* **101**, 253–258 (1997).
6. Colmati, F. *et al.* Surface structure effect on the electrochemical oxidation of ethanol on platinum single crystal electrodes. *Faraday Discuss.* **140**, 379–397 (2008).
7. Wang, J. T., Wasmus, S. & Savinell, R. F. Evaluation of ethanol, 1-propanol, and 2-propanol on a direct oxidation polymer-electrolyte fuel cell. A real-time mass spectrometry study. *J. Electrochem. Soc.* **142**, 4218–4224 (1995).
8. Xia, X. H., Liess, H. D. & Iwasita, T. Early stages in the oxidation of ethanol at low index single crystal platinum electrodes. *J. Electroanal. Chem.* **437**, 233–240 (1997).
9. Wang, Q. *et al.* Adsorption and oxidation of ethanol on colloid-based Pt/C, PtRu/C and Pt₃Sn/C catalysts: In situ FTIR spectroscopy and on-line DEMS studies. *Phys. Chem. Chem. Phys.* **9**, 2686–2696 (2007).
10. Wang, H., Jusys, Z. & Behm, R. J. Ethanol electro-oxidation on carbon-supported Pt, PtRu and Pt₃Sn/C catalysts: A quantitative study. *J. Power Sources* **154**, 351–359 (2006).
11. Adzic, R. *et al.* US Patent Application No. 20070264189 (2007).
12. Zhang, J. L. *et al.* Mixed-metal Pt monolayer electrocatalysts for enhanced oxygen reduction kinetics. *J. Am. Chem. Soc.* **127**, 12480–12481 (2005).
13. Batzill, M. & Diebold, U. The surface and materials science of tin oxide. *Prog. Surf. Sci.* **79**, 47–154 (2005).
14. Lindan, P. J. D. Water chemistry at the SnO₂(111) surface: The role of inter-molecular interactions and surface geometry. *Chem. Phys. Lett.* **328**, 325–329 (2000).
15. Trasatti, S. in *Interfacial Electrochemistry—Theory, Experiment, and Applications* (ed. Wieckowski, A.) 769–788 (Dekker, 1999).
16. Frenkel, A. Solving the 3D structure of metal nanoparticles. *Z. Kristallogr.* **222**, 605–611 (2007).
17. Nashner, M. S., Frenkel, A. I., Adler, D. L., Sharpeley, J. R. & Nuzzo, D. Structural characterization of carbon-supported platinum-ruthenium nanoparticles from the molecular cluster precursor PtRu₅C(CO)₁₆. *J. Am. Chem. Soc.* **119**, 7760–7771 (1997).
18. Willsau, J. & Heitbaum, J. Elementary steps of ethanol oxidation on Pt in sulfuric-acid as evidenced by isotope labeling. *J. Electroanal. Chem.* **194**, 27–35 (1985).
19. Shao, M. & Adzic, R. R. Electrooxidation of ethanol on a Pt electrode in acid solutions: In situ ATR-SEIRAS study. *Electrochim. Acta* **50**, 2415–2422 (2005).
20. Wieckowski, A., Sobkowski, J., Zelenay, P. & Franaszczuk, K. Adsorption of acetic acid on platinum, gold and rhodium electrodes. *Electrochim. Acta* **26**, 1111–1119 (1981).
21. Mavrikakis, M. & Barteau, M. A. Oxygenate reaction pathways on transition metal surfaces. *J. Mol. Catal. A* **131**, 135–147 (1998).
22. Idriss, H. Ethanol reaction over the surfaces of noble metal/cerium oxide catalysts. *Platinum Metals Rev.* **48**, 105–115 (2004).
23. Scott-Jones, G., Mavrikakis, M., Barteau, M. A. & Vohs, J. M. First synthesis, experimental and theoretical vibrational spectra of an oxametallacycle on a metal surface. *J. Am. Chem. Soc.* **120**, 3196–3204 (1998).
24. Batista, E. A. M., Motheo, G. R. P. & Iwasita, A. J. New mechanistic aspects of methanol oxidation. *J. Electroanal. Chem.* **571**, 273–282 (2004).
25. Wang, J. X., Marinković, N. S., Zajonz, H., Ocko, B. M. & Adzic, R. R. In situ X-ray reflectivity and voltammetry study of Ru(0001) surface oxidation in electrolyte solutions. *J. Phys. Chem.* **105**, 2809–2814 (2001).
26. Jiang, L. *et al.* Size-controllable synthesis of monodispersed SnO₂ nanoparticles and application in electrocatalysts. *J. Phys. Chem. B* **109**, 8774 (2005).
27. Bradely, D. An all-electron numerical method for solving the local density functional for polyatomic molecules. *J. Chem. Phys.* **92**, 508 (1990).

Acknowledgements

This work was carried out at Brookhaven National Laboratory under Contract No. DE-AC02-98CH10886 with the US Department of Energy, Office of Science, and supported by its Division of Chemical Sciences, Geosciences and Biosciences and its Division of Materials Sciences and Engineering, within the Office of Basic Energy Sciences. Part of the calculations were performed using the supercomputing facility at Center for Functional Nanomaterials of Brookhaven National Laboratory. A.I.F. acknowledges financial support by the DOE BES grant No. DE-FG02-03ER15476. Work at the NSLS was supported by the DOE BES grant DE-FG02-03ER15688

Additional information

Supplementary Information accompanies this paper on www.nature.com/naturematerials. Reprints and permissions information is available online at <http://npg.nature.com/reprintsandpermissions>. Correspondence and requests for materials should be addressed to R.R.A.